Supporting Information

Rapid *in vitro* assessment of *Clostridioides difficile* inhibition by probiotics using dielectrophoresis to quantify cell structure alterations

John H. Moore[1,#], Carlos Honrado[1,#], Victoria Stagnaro[3], Glynis Kolling[3], Cirle A. Warren[2], Nathan S. Swami[1,4*]

1 – Electrical & Computer Eng, University of Virginia, Charlottesville, Virginia-22904, USA

2 – Infectious Diseases, School of Medicine, University of Virginia, Virginia-22904, USA

3 – Biomedical Engineering, University of Virginia, Charlottesville, Virginia-22904, USA

4 – Chemistry, University of Virginia, Charlottesville, Virginia-22904, USA

 # Authors contributed equally

** Corresponding Author. Fax: +1-434-924-8818. Email: nswami@virginia.edu*

Pages: S1-S8 (8), Figures: S1-S4 (4), Tables: S1-S2 (2)

* Corresponding Author. Fax: +1-434-924-8818.

Email: nswami@virginia.edu

S1. Probiotic Coculture and Microbiological Analysis of *C. difficile*

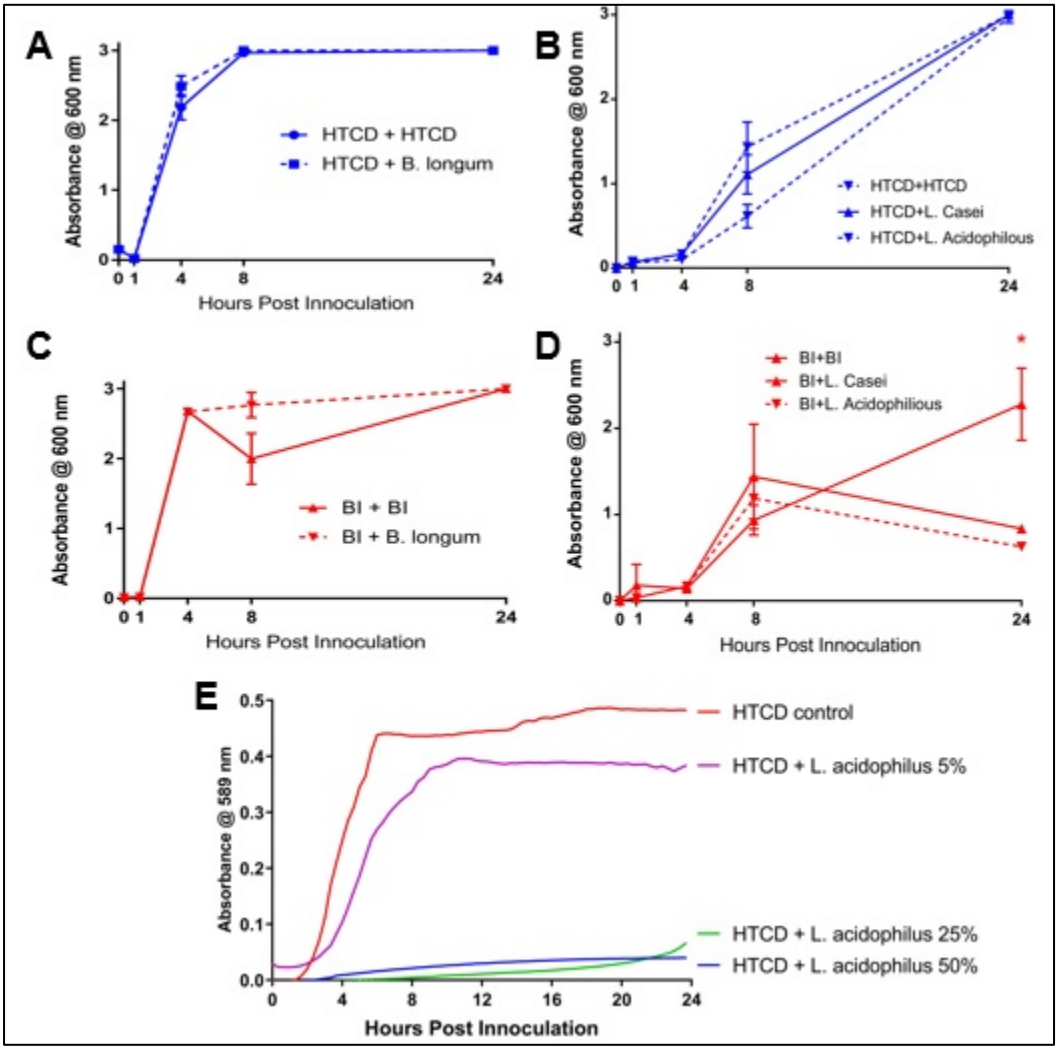

Fig. S1. Optimization of probiotic coculture model: A-D: Transwell coculture of probiotics with HTCD and BI. A transwell coculture was set up where both the probiotic strain and a *C. difficile* strain were cultured on different sides of a transwell coculture plate at 1/100 dilution from a culture at 1.0 absorbance at 600 nm in BHI media. The transwell membrane contained 0.2 micron pores, enough to prevent physical interaction between the cultures but enough to allow for metabolite exchange. Absorbance at 600 nm of the *C. difficile* strains was taken at select timepoints to measure growth. Metabolite concentrations at baseline were not enough to prevent growth of HTCD when cultured with *B. longum, L. casei, or L. acidophilus* after 24 hours, while the BI strain was growth inhibited only after 24 hours with *L. casei* and *L. acidophilus.* Because of the amount of time it took for the *Lactobacillus* strains to exhibit any inhibition of *C. difficile* and only in one of the two strains tested, we surmised it was probably because inhibitory metabolites from these cultures were not able to outpace *C. difficile* growth. **E:** Inhibition of HTCD using different levels of probiotic supernatant. Different levels of probiotic supernatant were combined with 50% BHI and a remaining amount of PBS. HTCD was growth inhibited with 25 and 50% but not significantly at 5% *L. acidophilus* supernatant (Two-way anova with Sidak's post-test).

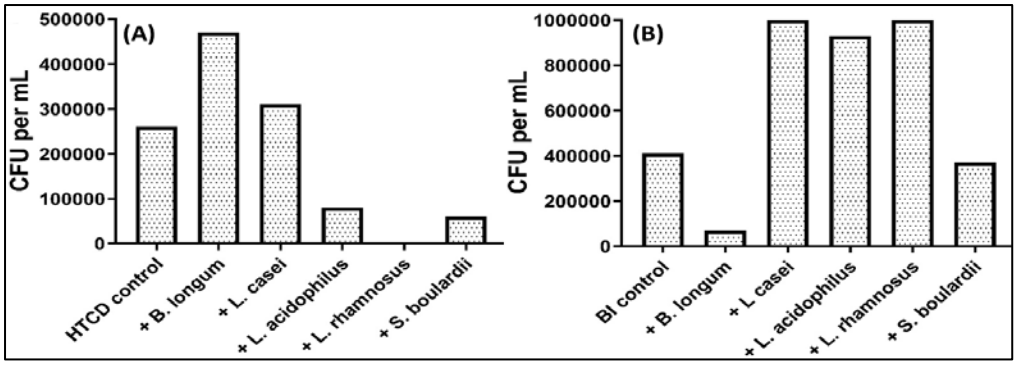

Fig. S2: HTCD and BI host cell adhesion following 24 hours of probiotic supernatant coculture: Host cell adhesion assay using Caco-2 cells to assess C. difficile of HTCD (A) and BI strain (B) after coculture with the indicated probiotic supernatants.

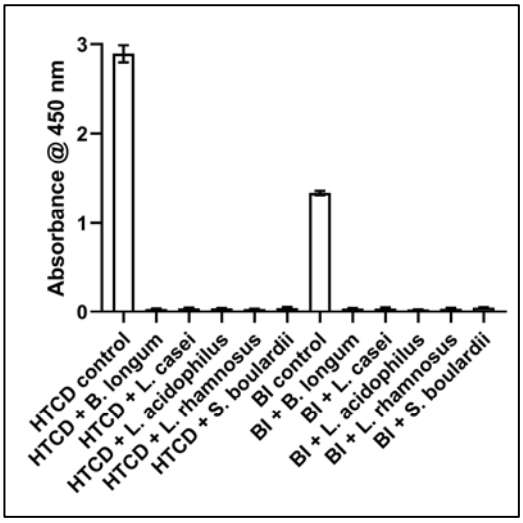

Description: A *C. difficile* toxin A/B ELISA was performed to examine changes in toxin production following coculture. HTCD and BI controls differed slightly from previous controls in that fresh BHI was added in equal parts to sterile PBS instead of spent HTCD or BI media, since this would already contain toxin. Interestingly, all coculture supernatants significantly suppressed toxin production after 24 hours of culture (Oneway ANOVA with Tukey's multiple comparisons post-test, $p<0.05$ in all cases). While *B. longum* and *S. boulardii* did not inhibit growth following coculture; they inhibited toxin secretion, suggesting other methods by which probiotics can confer protection against *C. difficile* pathogenicity.

Fig. S3: Toxin ELISA of HTCD and BI cultures following probiotic coculture

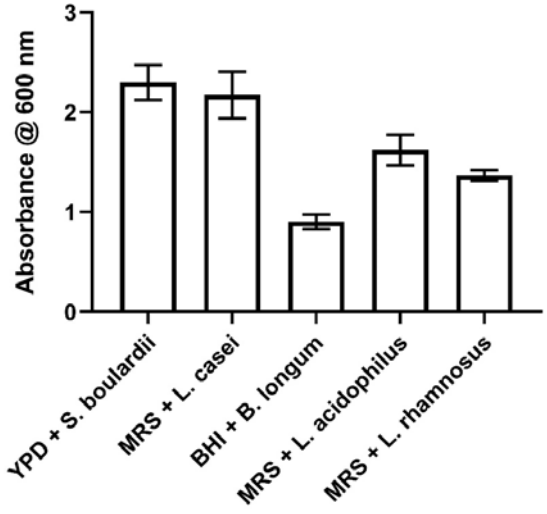

Figure S4: OD600nm measurement of each probiotic strain after 48 hours in triplicate (separate cultures)

S2: Fitting *C. difficile* DEP spectra to the ellipsoidal double-shell model:

Dielectrophoresis Overview

i. Theoretical Background

AC electrokinetics can be employed to induce movement and/or rotation of particles subjected to an AC electric field. In general, cells do not hold fixed dipole moments, but can be induced to form a dipole by interfacial polarization. This is due to the accumulation of charge at the interface between medium and cell. If the AC electric field is spatially non-uniform, dielectrophoresis (DEP) exerts a frequency-selective force on the dipole, causing movement of the cell.. The time averaged DEP force ($\langle \mathbf{F}_{DEP} \rangle$) on a particle is given by:

$$\langle \mathbf{F}_{DEP} \rangle = 2\pi\, \varepsilon_{medium}\, r^3\, \mathrm{Re}\left[\tilde{f}_{CM}\right] \nabla |\mathbf{E}|^2 \qquad \text{Eq. (S1)}$$

with $\tilde{f}_{CM}$ referring to the Clausius-Mossotti factor:

$$\tilde{f}_{CM} = \frac{\tilde{\varepsilon}_{particle} - \tilde{\varepsilon}_{medium}}{\tilde{\varepsilon}_{particle} + 2\tilde{\varepsilon}_{medium}} \qquad \text{Eq. (S2)}$$

where r is the radius of the particle, $\mathrm{Re}\left[\tilde{f}_{CM}\right]$ the real part of the Clausius-Mossotti factor and $\mathbf{E}$ the electric field. If the electric field is uniform, the gradient of the magnitude of the field is zero ($\nabla |\mathbf{E}|^2 = 0$), which means that there is no DEP force. Also, the r^3 term means the time averaged force is proportional to particle volume.

$\tilde{\varepsilon}_{medium}$ and $\tilde{\varepsilon}_{particle}$ are the complex permittivities of the medium and particle, respectively, and represent the frequency dependence of the material permittivity. They are given by:

$$\tilde{\varepsilon}_{medium} = \varepsilon_0 \varepsilon_{medium} - i\frac{\sigma_{medium}}{\omega} \qquad \text{Eq. (S3)}$$

$$\tilde{\varepsilon}_{particle} = \varepsilon_0 \varepsilon_{particle} - i\frac{\sigma_{particle}}{\omega} \qquad \text{Eq. (S4)}$$

where ε_0 is the constant vacuum permittivity (8.85×10^{-12} F m^{-1}), ε_{medium} and $\varepsilon_{particle}$ are the dimensionless numbers referring to the relative permittivity of the medium and particle, respectively, and σ_{medium} and $\sigma_{particle}$ are the conductivities (S m^{-1}) of the medium and particle, respectively.

The Clausius−Mossotti factor ($\tilde{f}_{CM}$) is a frequency-dependent measure of cell polarizability dictating force direction. For particles less polarizable than the medium, *i.e.*, $\mathrm{Re}\left[\tilde{f}_{CM}\right] < 0$, negative DEP (nDEP) occurs, with particles being repelled from the regions of high field strength. When $\mathrm{Re}\left[\tilde{f}_{CM}\right] > 0$, particles are in turn more polarizable than the medium, thus positive DEP (pDEP) ensues, with the particles moving to areas of higher electric field strength [1], [2].

ii. Quantification of the DEP Force

The velocity of cells within the DEP system is tracked and analyzed to quantify the DEP force enacting on cells [3], [4]. DEP spectral measurements were conducted on a 3DEP dielectrophoretic analyzer (DepTech, UK). The non-uniform electric field is applied to gold-plated electrode stripes inside the wall of individual chambers. The relative DEP force at each frequency is obtained by analyzing spatio-temporal variations in light intensity from particle scattering after normalizing against the background at zero field ($\nabla |\mathbf{E}|^2 = 0$), after accounting for the field profile [5], [6]. The trajectory of cells within the chamber is recorded at high frame rate. Using Newton's second law, for a particle of mass m, the net dielectrophoeretic force F_{DEP} on the accelerated particle of radius r, within a medium of viscosity η, can be determined by tracking its displacement x as a function of time t to obtain $(\mathrm{d}x/\mathrm{d}t)$ and $(\mathrm{d}^2x/\mathrm{d}t^2)$ for each population analyzed. Thus, the relative DEP force can be approximated using:

$$F_{DEP} - 6\pi\eta r\frac{\mathrm{d}x}{\mathrm{d}t} = m\frac{\mathrm{d}^2x}{\mathrm{d}t^2} \qquad \text{Eq. (S5)}$$

The DEP response is measured at 14 different frequencies (from approximately 20 kHz to 45 MHz) applied independently within separate wells. In this manner, the relative DEP force for each sample can be estimated along the frequency spectrum.

iii. Multi-shell Modelling

For the case where a particle is suspended in a dielectric medium, dielectric theory can be used to estiamte the dielectric properties of the suspension [7]. This mixture of particle and medium can be approximated to that of a single dispersion using Maxwell's mixture theory (MMT) [8]. For the case of a particle (such as a mammalian cell or bacterium) in suspending medium, MMT can be used to define the dielectric properties of said particle [2], [8]. MMT-based, multi-shell models have been used to retrieve the dielectric properties of various particles [9]–[12].

The ellipsoidal model represented in Fig. 3a, is the most widely used approximation for non-spherical particles such as bacteria [2], [13]–[16]. In this model, a dielectric particle is modelled with semi-axes $n = a, b$ and c, which for a prolate spheroid such as *C. difficile* bacterium are $a > b = c$ (Fig. 3b). While bacteria have an intricate internal structure, surrounded by a thick wall and membrane, a simpler approximation can be used where a two-shell model is applicable (Fig. 3b). In this model, there are three dispersions, corresponding to each of the existing interfaces between each layer: medium / wall (subscripts 3 & 2), wall / membrane (subscripts 2 & 1) and membrane / interior (subscripts 1 & 0). Due to the configuration of the 3DEP wells used in the experiments, the electric field causes ellipsoidal particles to orient with their major axis a parallel to the electric field (x direction) [17]. Thus, the DEP force acting on the particle is given by:

$$\langle \mathbf{F}_{DEP} \rangle = 2\pi\, \varepsilon_{medium}\, abc\, \mathrm{Re}\left[\widetilde{K}_{a,3/2}\right] \nabla|\mathbf{E}|^2 \qquad \text{Eq. (S6)}$$

where $\widetilde{K}_{a,3/2}$ is the dipole coefficient (analogous to the $\tilde{f}_{CM}$) along the major axis a at the final interface (medium / wall). This coefficient includes all the existing interfaces up to that point, and depends on the depolarizing factor $A_{a,3/2}$ and the complex permittivity up to that interface. It is calculated by:

$$\widetilde{K}_{a,3/2} = \frac{\tilde{\varepsilon}_{2/1} - \tilde{\varepsilon}_3}{3(A_{a,i}(\tilde{\varepsilon}_{2/1} - \tilde{\varepsilon}_3) + \tilde{\varepsilon}_3)} \qquad \text{Eq. (S7)}$$

$$A_{a,3/2} = \frac{1}{1-q^2} + \frac{q}{(1-q^2)^{3/2}} arcos(q) \qquad \text{Eq. (S8)}$$

where q is the ratio of semi-axis (a_2/b_2), while the complex permittivity up to each interface (for $i = 1$ and 2) is calculated through [16]:

$$\tilde{\varepsilon}_{i/i-1} = \tilde{\varepsilon}_i \frac{2\tilde{\varepsilon}_i + \tilde{\varepsilon}_{i-1} - 2v_i(\tilde{\varepsilon}_i - \tilde{\varepsilon}_{i-0})}{2\tilde{\varepsilon}_i + \tilde{\varepsilon}_{i-1} + v_i(\tilde{\varepsilon}_i - \tilde{\varepsilon}_{i-0})} \qquad \text{Eq. (S9)}$$

where v_i is the volume fraction at the i-th layer (for $i = 1$ and 2) calculated as $v_i = (1 - d_i/a_2)^3$, with d_i being the thickness of the i-th layer ($d_i \ll a_2$). By calculating $\mathrm{Re}\left[\widetilde{K}_{a,3/2}\right]$ it is possible to model the corresponding DEP behaviour of the particles by generating multiple polarization dispersions and fitting them to the experimental DEP data. The dispersion with the optimal fit thus gives the estimate of dielectric properties for a specific sample. Fig. 3C-F and Fig.3G-H show the dispersions and optimal fits, when possible, for 4h coculture samples and 1h coculture samples, respectively.

For the modelling process, the values of σ_{medium} and ε_{medium} are fixed at 10 mS m^{-1} and 78, respectively. Geometrical parameters were measured from microscopy images for 4h coculture samples and used as reference for the fitting process for 1h coculture samples. Wall and membrane thickness values were fixed based on literature values at 30 and 8 nm, respectively [2], [17]. The resultant fitted parameters are summarized in **Table S1** for 4h coculture samples and **Table S2** for 1h coculture samples.

Table S1: Two-shell model-derived dielectric parameters after 4h coculture

Parameter	HTCD Control I	HTCD *B. longum*	BI Control I	BI *B. longum*	HTCD Control II	HTCD *S. boulardii*	BI Control II	BI *S. boulardii*
Major axis (a) [m]	3.0×10^{-6}	3.1×10^{-6}	1.0×10^{-6}	1.2×10^{-6}	3.0×10^{-6}	2.1×10^{-6}	1.0×10^{-6}	1.4×10^{-6}
Minor axis (b, c) [m]	0.4×10^{-6}	0.4×10^{-6}	0.5×10^{-6}	0.5×10^{-6}	0.4×10^{-6}	0.6×10^{-6}	0.6×10^{-6}	0.5×10^{-6}
Wall permittivity (ε_{wall}) [1]	50	50	60	55	50	65	60	55
Wall conductivity (σ_{wall}) [S m^{-1}]	1.0×10^{-4}	8.0×10^{-5}	2.0×10^{-3}	2.0×10^{-3}	5.0×10^{-4}	1.0×10^{-4}	4.0×10^{-3}	1.0×10^{-3}
Membrane permittivity ($\varepsilon_{membrane}$) [1]	15	15	18	16	13	18	17	19
Membrane conductivity ($\sigma_{membrane}$) [S m^{-1}]	$<1.0 \times 10^{-7}$	$<1.0 \times 10^{-7}$	2.0×10^{-5}	3.0×10^{-5}	$<1.0 \times 10^{-7}$	$<1.0 \times 10^{-7}$	1.0×10^{-4}	1.0×10^{-4}
Interior permittivity ($\varepsilon_{interior}$) [1]	50	40	40	40	40	45	40	45
Interior conductivity ($\sigma_{interior}$) [S m^{-1}]	0.60	0.58	0.35	0.37	0.45	0.50	0.36	0.52

Square brackets denote units; 1 indicates dimensionless parameter.

Table S2: Two-shell model-derived dielectric parameters after 1h coculture

Parameter	**HTCD** **Control**	**BI** **Control**	**BI** ***L. acidophilus***	**BI** ***L. casei***	**BI** ***L. rhamnosus***
Major axis (a) [m]	2.9×10^{-6}	1.0×10^{-6}	1.1×10^{-6}	1.0×10^{-6}	1.0×10^{-6}
Minor axis (b, c) [m]	0.4×10^{-6}	0.5×10^{-6}	0.6×10^{-6}	0.6×10^{-6}	0.5×10^{-6}
Wall permittivity (ε_{wall}) [1]	50	60	50	55	50
Wall conductivity (σ_{wall}) [S m^{-1}]	5.0×10^{-5}	1.5×10^{-3}	3.0×10^{-3}	4.0×10^{-3}	5.0×10^{-3}
Membrane permittivity $(\varepsilon_{membrane})$ [1]	14	16	15	15	14
Membrane conductivity $(\sigma_{membrane})$ [S m^{-1}]	$<1.0 \times 10^{-7}$	2.0×10^{-5}	6.0×10^{-5}	9.0×10^{-5}	5.0×10^{-5}
Interior permittivity $(\varepsilon_{interior})$ [1]	50	40	25	30	20
Interior conductivity $(\sigma_{interior})$ [S m^{-1}]	0.60	0.35	0.26	0.27	0.20

Square brackets denote units; 1 indicates dimensionless parameter.

References

[1] Pohl, H. A., Crane, J. S. Dielectrophoresis of Cells. *Biophys. J.* **1971**, 11 (9), 711–727, 1971.

[2] Morgan, H., Green, N. G. *AC Electrokinetics: colloids and nanoparticles*. Baldock, Hertfordshire, UK: Research Studies Press Ltd., **2002**.

[3] Su, Y.-H., Tsegaye, M., Varhue, W., Liao, K. T., Abebe, L. S., Smith, J. A., Guerrant, R. L., Swami.. N. S. Quantitative dielectrophoretic tracking for characterization and separation of persistent subpopulations of Cryptosporidium parvum. *Analyst* **2014**, 139 (1), 66–73.

[4] Rohani, A. Moore, J. H., Kashatus, J. A., Sesaki, H., Kashatus, D. F., Swami, N. S. Label-Free Quantification of Intracellular Mitochondrial Dynamics Using Dielectrophoresis. *Anal. Chem.* **2017**, 89, 5757–5764.

[5] Broche, L. M., Hoettges, K. F., Ogin, S. L., Kass, G. E. N., Hughes, M. P. Rapid , automated measurement of dielectrophoretic forces using DEP-activated microwells. *Electrophoresis* **2011**, 32, 2393–2399.

[6] Rohani, A., Varhue, W., Su, Y.H., Swami, N. S. Quantifying spatio-temporal dynamics of biomarker pre-concentration and depletion in microfluidic systems by intensity threshold analysis. *Biomicrofluidics* **2014**, 8, 052009: 1–13.

[7] Pethig, R. *Dielectric and Electric Properties of Biological Materials*. John Wiley & Sons, 1979.

[8] Maxwell, J. C. *A treatise on electricity and magnetism*, vol. 1. Clarendon Press, 1881.

[9] Hanai, T., Koizumi, N., Irimajiri, A. A method for determining the dielectric constant and the conductivity of membrane-bounded particles of biological relevance. *Biophys. Struct. Mech.* **1975**, 1 (4), 285–294.

[10] Irimajiri, A., Hanai, T., Inouye, A. A dielectric theory of 'multi-stratified shell' model with its application to a lymphoma cell. *J. Theor. Biol.* **1979**, 78 (2), 251–269.

[11] Huang, Y., Hölzel, R., Pethig, R., Wang, X. B. Differences in the AC electrodynamics of viable and non-viable yeast cells determined through combined dielectrophoresis and electrorotation studies. *Phys. Med. Biol.* **1992**, 37 (7), 1499–1517.

[12] Wang, X. B., Huang, Y., Gascoyne, P. R. C., Becker, F. F., Hölzel, R., Pethig, R. Changes in Friend murine erythroleukaemia cell membranes during induced differentiation determined by electrorotation. *BBA - Biomembr.* **1994**, 1193 (2), 330–344.

[13] Gimsa, J., Müller, T., Schnelle, T., Fuhr, G. Dielectric spectroscopy of single human erythrocytes at physiological ionic strength: dispersion of the cytoplasm. *Biophys. J.* **1996**, 71 (1), 495–506.

[14] Asami, K. Yonezawa, T. Dielectric behavior of non-spherical cells in culture. *BBA - Gen. Subj.* **1995**, 1245 (3), 317–324.

[15] Miller, R. D., Jones, T. B. Electro-orientation of ellipsoidal erythrocytes. Theory and experiment. *Biophys. J.* **1993**, 64 (5), 1588–1595.

[16] Fernandez, R. E., Rohani, A., Farmehini, V., Swami, N. S. Review: Microbial analysis in dielectrophoretic microfluidic systems. *Anal. Chim. Acta* **2017**, 966, 11–33.

[17] Su, Y. H., Rohani, A., Warren, C. A., Swami, N. S. Tracking Inhibitory Alterations during Interstrain Clostridium difficile Interactions by Monitoring Cell Envelope Capacitance. *ACS Infect. Dis.* **2016**, 2 (8), 544–551.